

TRISTAR: Triple-Signal Stair Recognition and Vision-Only Indoor Navigation for Search-and-Rescue Micro-UAVs

Octavian Gîngu* and Stelian Spînu†

Military Technical Academy “Ferdinand I”, Bucharest, Romania

*octavian.gingu@mta.ro

†stelian.spinu@mta.ro

Abstract—Indoor search-and-rescue (SAR) operations often require rapid situational awareness where GNSS signals are unavailable and human access is difficult or hazardous. While most autonomous aerial systems rely on LiDAR, stereo vision, or specialized depth cameras, such solutions increase both hardware complexity and deployment costs. This paper presents a complete autonomous indoor navigation framework for low-cost unmanned aerial vehicles based exclusively on monocular vision. Implemented on a DJI Tello platform, the system combines monocular depth estimation using Depth Anything V2 with classical computer vision and lightweight deep learning models for scene understanding, victim detection, and hazard recognition. The framework consists of two independent behaviors: (i) corridor exploration with automatic door detection, room entry, OCR-based room identification, and victim inspection; and (ii) autonomous stair ascent based on TRISTAR (TRI-Signal Stair Ascent Recognition), a novel triple-sensor fusion method that integrates structural cues (Sobel filtering), texture analysis (multi-scale Gabor filtering), and geometric depth from monocular depth estimation. Evaluation used real indoor flights in a university building. Depth calibration reduced relative depth error from 27.4% to below 10%, while the door detection algorithm reached a precision of 0.93 and an F1-score of 0.91. A dedicated ablation study shows that multi-sensor fusion significantly improves stair-recognition robustness compared to individual sensing modalities, and a failure-case analysis delineates the limits of monocular perception under challenging lighting and reflective surfaces. The results demonstrate that reliable indoor exploration and stair traversal are achievable on resource-constrained platforms without specialized ranging hardware—a practical, cost-effective solution for rapid SAR deployment.

Index Terms—autonomous drones, indoor navigation, search and rescue, monocular depth estimation, stair detection, sensor fusion, computer vision, UAV autonomy.

I. INTRODUCTION

Indoor search-and-rescue (SAR) is, alongside urban rescue, one of the most demanding classes of first-response intervention. Unlike operations conducted in open space, indoors the rescuers have no satellite positioning, visibility is degraded by dust, smoke, or darkness, and the building layout is seldom known in advance. Under such conditions, every additional minute spent locating the people inside sharply increases the risk to victims and rescuers alike. Public statistics confirm the scale of the problem: in Romania alone, residential-building fires exceed 6,900 cases per year, complemented by thousands

of in-building emergency-medical interventions,¹ a significant fraction of which involve spaces with difficult access or reduced visibility. At the same time, data from FEMA and NIST indicate that the critical time window for rescuing a trapped victim is on the order of minutes, while the average time for a specialized team to penetrate an unknown building remains well above that value. This gap justifies the continued investment in technologies that give teams an informational head start before they physically enter.

Small unmanned aerial vehicles (micro-UAVs) have become an increasingly attractive option for this class of missions, thanks to their ability to rapidly inspect narrow spaces without exposing human personnel. Yet ordinary commercial drones remain fundamentally dependent on a trained operator, and their real indoor autonomy is limited: in the absence of GNSS, most industrial solutions resort to additional sensors (LiDAR, stereo depth cameras, high-grade IMUs) that substantially increase the cost, mass, and complexity of the system. Current commercial offerings fall broadly into two categories. On one side are industrial drones such as Skydio or the professional DJI series (Matrice, Mavic 3 Enterprise), which are capable but costly (from 4,000 to over 25,000 EUR) and dependent on dedicated ranging hardware. On the other side are lightweight platforms that expose a programmatic API but, lacking a depth sensor, restrict their real autonomy to point tasks such as face tracking or reactive obstacle avoidance. Neither category directly covers the use case addressed here: a low-cost drone able to autonomously explore a corridor, enter a room, scan it, and report—something that, to date, has required either a human operator or an expensive sensor suite.

Recent advances in monocular vision reopen this problem from a software-centric angle. Transformer-based models for monocular depth estimation now yield reasonably accurate metric depth directly from an ordinary video stream, without a stereo rig or a LiDAR unit. In particular, Depth Anything V2 [1], trained on diverse indoor and outdoor data, produces per-pixel depth at a latency compatible with a real-time control loop on a commodity GPU. If monocular depth is good enough to estimate the distance to a wall, then it should also be

¹General Inspectorate for Emergency Situations (IGSU), *Evaluation of IGSU activity in 2024*.

good enough to let a drone navigate a corridor autonomously and identify an open door. Building on this observation, our work extracts as much navigation- and reporting-relevant information as possible from a single video feed, instead of adding hardware to the drone. The solution is built on a DJI Tello—accessible (list price under 150 EUR) and, although not designed for complex autonomous flight, exposing an SDK sufficient to issue remote-control commands at useful rates (10–12 Hz).

Beyond navigation proper, a realistic search mission entails complementary tasks: identifying the rooms the drone enters (by reading the door number), detecting people and estimating their condition (to dispatch the appropriate medical team), and flagging visible hazards (fire, smoke). Dedicated neural models already exist for each of these; the real challenge is not the models themselves but their coherent integration into a system that operates without continuous human intervention for the entire mission. The system is organized as a local server with a web interface, letting the operator trigger and monitor the mission in real time without directly piloting the drone. It supports two distinct autonomous behaviors—corridor navigation and stair ascent—each implemented as a separate module, individually validatable and triggered from the operator interface according to the mission scenario.

Contributions. The main contributions of this paper are summarized as follows.

- 1) A **complete autonomous indoor-navigation system for low-cost drones based exclusively on monocular perception**, with no specialized depth sensors, integrating depth estimation, autonomous navigation, semantic scene analysis, and automatic operational reporting into a single functional chain around one onboard camera feed.
- 2) **TRISTAR** (TRI-Signal STair Ascent Recognition), a **multi-sensor stair detector** that fuses structural, textural, and geometric information obtained from Sobel filters, multi-scale Gabor filters, and monocular depth estimation into a single composite confidence score.
- 3) An **appearance-free door-detection algorithm based on scene geometry and a calibrated depth map**, requiring no dedicated trained detector, robust to appearance traps, and functional even when the door is only partially in view.
- 4) A **dynamically switchable empirical depth-calibration scheme** (room/corridor profiles) that reduces the relative monocular depth error from 27.4% to below 10%, enabling reliable control decisions without a ranging sensor.
- 5) A **real-flight validation and ablation study** that quantifies the contribution of each virtual sensor to the performance of the TRISTAR detector.
- 6) A **systematic failure-case analysis** exposing the specific limitations of monocular perception in complex indoor environments (reflective surfaces, glazing, low light).

The implementation discussed in this paper is publicly available on GitHub at the following repository: <https://github.com/tavingingu/HawkOps-Indoor-Drone-Navigation-and-TRISTAR-Stair-Climbing>.

II. RELATED WORK

Autonomous navigation with small drones has advanced rapidly, both through commercial products and through academic contributions. We review the solutions relevant to our use case—autonomous indoor exploration from a monocular video feed—and identify the limitations that motivate our approach.

A. Commercial drone platforms

Skydio [2] (Skydio 2+ / X10) is among the best-known makers of autonomous drones, capable of avoiding obstacles even in cluttered spaces thanks to six 4K stereo cameras and an onboard NVIDIA Jetson processor. However, the starting price of a Skydio X10 exceeds 11,000 USD, the solution is entirely black-box with no SDK to extend the navigation logic, and the supported missions are limited to manufacturer-defined behaviors (tracking, patrol). **DJI** professional models [3] (Matrice 30/350 RTK) carry stereo cameras and ToF sensors and support *ActiveTrack/Waypoint* modes outdoors, but an equipped Matrice 30 exceeds 9,000 EUR, indoors without GNSS it falls back on a Vision Positioning System that demands adequate lighting and floor texture, and there is no native mode for entering rooms or reading door labels. **Modal AI** [4] (Starling 2 with Voxl 2) targets developers with a ROS/PX4 stack and monocular SLAM, but a starter kit costs about 5,500 USD, requires PX4/ROS expertise, and provides no autopilot for complex “explore the corridor and enter each room” missions. Finally, the **DJI Tello** educational drone (~80 g, under 150 EUR) exposes a UDP SDK abstracted by the open-source `djitellopy` [5] library; it carries no dedicated depth sensor—its only external signal is a 720p frontal video stream—which makes it an attractive research platform precisely because any behavioral improvement is a consequence of the software layer above the SDK, and is therefore directly portable and reproducible.

B. Monocular depth estimation

Estimating depth from a single image is a classic problem accelerated by transformer models trained on diverse datasets. **MiDaS** [6] popularized scale-invariant relative depth from a single image but produces only relative depth. **ZoeDepth** [7] adds a metric regression head (trained on NYUv2 [8] and KITTI [9]) yet its GPU latency can be prohibitive for real-time loops above 10–15 Hz. **Depth Anything V2** [1], adopted in this work, is pretrained on a large volume of synthetic data and fine-tuned on real data; with a ViT-S backbone it runs above 20 Hz at 360p on a consumer GPU and, crucially, exhibits markedly better temporal stability on video than MiDaS or ZoeDepth—essential for stable door and step detection. Its relative output is converted to metric distances through an empirical calibration built on real scenes (Section III-B), which proved more stable on the specific geometry of the targeted corridors and rooms than a pretrained metric variant.

C. Academic prototypes and structure detection

A first group of works uses monocular depth (MiDaS, Depth Anything) for reactive obstacle avoidance on drones, but without high-level logic (room entry, label reading, reporting). A related current is neural monocular SLAM (DROID-SLAM [10], DPVO [11]), which reconstructs a globally consistent 3D map—a more ambitious goal than the frame-by-frame reactive navigation we pursue, and one whose online computational cost remains high for a 10–12 Hz loop on a small commercial drone. Door detection has been addressed with RGB-D data: Arduengo et al. [12] operate doors with a mobile robot, estimating the parameters needed for autonomous opening, while Ramôa et al. [13] build an RGB-D dataset and classify door state on a low-power device; both rely either on dedicated depth sensors or on models trained on the visual appearance of the door. YOLO-based door detectors [14], [15] work reasonably on static images but are unstable on moving video and are fundamentally unsuited to our central case—an *open* door the drone flies through: as the drone approaches, the door frame, threshold, and handle leave the field of view, leaving an appearance-trained detector with no cues. In essence, our system does not detect a door as an object, but a structural opening in an otherwise flat wall—a more distant region surrounded by nearby surfaces—a configuration described far more naturally through the depth map than through an appearance model. Autonomous stair ascent by drones is addressed only occasionally, typically with LiDAR, stereo, or fiducial markers, with purely monocular solutions being rare and limited to simple demonstrators. Integrated indoor SAR systems appear at events such as the DARPA Subterranean Challenge [16], but these use industrial-grade drones with LiDAR and additional sensors, at a total platform cost far above that of an accessible, low-cost system.

For the detection of regular structures (stair steps), our work leans on established classical techniques. The Sobel operator yields a directional gradient whose vertical modulus $|G_y|$ responds strongly to each horizontal step edge, forming a 1D profile of regular peaks. Gabor filters [17], orientation-selective at $\theta = 90^\circ$ and tuned to several wavelengths, respond much more strongly to horizontal lines (steps) than to vertical ones (doors, railings). The Hough transform would be a natural alternative but tends to produce many false positives on partially occluded steps or under strong perspective; we therefore prefer the Sobel/Gabor combination, complemented by a third virtual sensor derived from the depth map.

D. Positioning

Table I summarizes the functional comparison against the most representative commercial and academic solutions. To the best of our knowledge, none of the studied commercial systems covers, without additional programming effort, all four critical capabilities—corridor navigation with automatic room entry, autonomous stair ascent, OCR label reading, and AI-based medical assessment of detected people—which the proposed system delivers starting from a drone costing under 150 EUR, with spatial perception that is exclusively

TABLE I: Functional comparison of existing solutions and the proposed system.

Capability	Skydio X10	DJI Matrice 30	Modal AI Starling	Tello + lib.	Proposed
HW cost (EUR)	>11k	>9k	~5.5k	<150	<150
Hardware depth sensor	✓	✓	✓	–	–
Open SDK	~	✓	✓	–	–
Indoor nav. (no GNSS)	✓	~	✓	–	✓
Autonomous room entry	–	–	code	code	✓
OCR label reading	–	–	code	code	✓
Autonomous stair ascent	–	–	code	code	✓
Person + AI triage	~	~	code	code	✓
Post-mission report	–	~	code	code	✓

✓: supported; ~: partial; –: absent; “code”: requires full user implementation.

monocular. The design trade-offs implied by these choices (no global map, strict separation of the two behaviors) are stated explicitly and analyzed in Section V.

III. METHODS

A. System architecture

The system is organized as five components communicating over REST and WebSocket on the local network: a **backend** (FastAPI [18] plus vision models), a **web frontend** (React), **two external microservices** (OCR and medical AI) called on demand, the **DJI Tello** drone (connected by UDP), and a **database** that persists missions and results (Fig. 1). The backend is the core: `server.py` mounts the endpoints and manages the drone lifecycle; `tello_controller` wraps `djitellopy` behind a stable API; `stream_pipeline` captures frames and runs Depth Anything V2; the `navigation` package holds the corridor logic; and `navigation/stair_climber` holds the fully independent stair module. The pipeline runs three neural models concurrently on GPU—Depth Anything V2 (ViT-S) for depth, YOLO11n-Pose [19] for people and 17 body keypoints, and YOLOv8 [20] for fire/smoke—alongside video decoding and the autopilot, in distinct Python threads. Two microservices with heavy dependencies are isolated: OCR (EasyOCR [21]) and medical AI (Gemini 2.5 Flash [22]); both are optional for navigation and can be disabled when offline. The total size of the locally loaded models is ≈ 200 MB.

Several challenges shaped these design decisions. The Tello control channel accepts `send_rc_control(lr,fb,ud,yaw)` commands only at 10–15 Hz over UDP; the H.264 video stream introduces 80–150 ms of decoding latency; and, on a moving drone, the metric depth of Depth Anything V2 can oscillate by ± 0.2 m between consecutive frames, especially on homogeneous surfaces. To avoid unstable state switching, all derived metrics are smoothed by an exponential moving average (EMA); phase transitions additionally apply a symmetric *deadband* around the target value and accept a new state

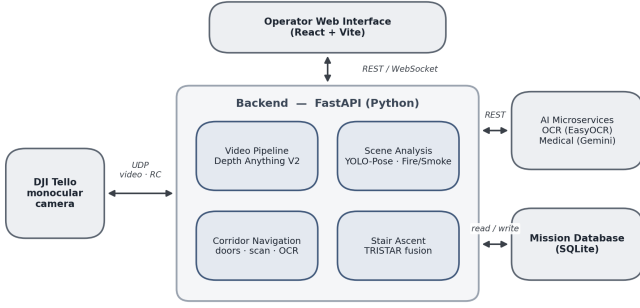


Fig. 1: Overall system architecture. The FastAPI backend runs all perception locally (monocular depth, corridor navigation, TRISTAR stair ascent, scene analysis) and communicates with the operator web interface, the DJI Tello, a mission database, and two optional AI microservices (OCR, medical) that can be disabled when there is no connectivity.

only after the EMA metric stays within the band for several consecutive cycles (`stable_hits= 3`), which eliminates the pendular transitions caused by frame-to-frame fluctuations. Because a control error has physical consequences, each phase has a timeout, a low-battery forced-landing condition, an operator abort button, and guard-clause checks at the start of every control loop.

B. Video pipeline and depth calibration

A dedicated thread reads the last decoded frame from the SDK at a target of 30 FPS and places it into a bounded, drop-oldest queue: in real time, only the latest frame matters. Depth Anything V2 (ViT-S) is loaded from a local checkpoint and, in the configuration used here, runs the *relative* variant; the relative map is converted to metric distances by an empirical calibration layer, which grants full control over the correspondence between the model’s raw value and the true distance and adapts it to the targeted geometry.

The calibration is a lookup table mapping the raw value (blue-channel luminance of the colored map, 0–255) to the real distance measured with a laser rangefinder, interpolated linearly. It is organized into dynamically switchable *profiles*: `room` (a furnished room) and `corridor` (a long hallway with plain walls). Profiles are switched mid-mission through a REST endpoint—the corridor autopilot switches to `room` after crossing a door and back to `corridor` on exit. From the calibrated map, per-frame global metrics feed both the autopilot and the interface, the most important being the global coefficient of variation (CoV) and the “blue ratio”:

$$\text{CoV} = \frac{\sigma(D)}{\mu(D)}, \quad r_{\text{blue}} = \frac{|\{p \in D \mid d_{\min} \leq D(p) \leq d_{\max}\}|}{|D|}, \quad (1)$$

where D is the set of per-pixel metric depths. Steps produce a large CoV; a flat wall a small one. The blue ratio acts as

a proxy for how “far” the scene extends and is central to the door-distance control loop.

C. Corridor navigation

The corridor module explores a hallway and enters each open room in turn. The drone’s primary motion is a *lateral crab to the right*: it keeps a constant yaw and sweeps the corridor searching for an open door, then runs a sequence of phases—centering, distance control, entry, scan, and exit—before resuming the crab to find the next door.

1) *Door detection*: Door detection uses *only* the depth map, a deliberate choice justified by the intrinsically spatial nature of an open door: it appears as a region significantly more distant than the surrounding walls. A binary mask keeps pixels between 1.7 m and 6.0 m; morphological *closeopen/dilate* operations with a 7×7 structuring element consolidate contours; contours are extracted and each candidate is filtered by three successive tests. The *shape* filter requires at least four vertices, a width/height ratio in $[0.35, 2.0]$, a height of at least 30% of the frame, and a contour spanning from the top toward the bottom. The *content* filter requires fewer than 50% of the candidate’s pixels to be closer than 1.5 m: an open door is an opening, not a nearby surface. The *vertical-edge* filter is the most important: on the candidate’s depth ROI, the horizontal gradient $|G_x|$ at the left and right margins must be significantly stronger than in the center. Concretely, with $Q_{0.9}$ the 90th percentile of $|G_x|$,

$$R = \frac{Q_{0.9}(|G_x|_{\text{margin}})}{Q_{0.9}(|G_x|_{\text{center}})} \geq 1.20, \quad (2)$$

must hold (a single valid edge suffices, at a stricter $R \geq 1.45$, when the door touches the frame border). This exploits the fact that an open door is framed by the door casing, which produces strong vertical edges in the depth map. Among the survivors, the candidate maximizing $R \times \text{area}$ is selected (Fig. 2).

2) *Centering, distance control and entry*: Once a door is detected, the drone aligns its frontal axis with the door axis through a proportional lateral loop with a deadband, $v_{lr} = \text{clip}(K_{lr}(x_{\text{door}} - x_{\text{center}}), -v_{\max}, +v_{\max})$, with $K_{lr} \approx 0.10$ and a ~ 25 px tolerance, issued as short pulses with pauses to let the drone settle. Distance is then regulated using `full_frame_blue_ratio`, whose interpretation is counter-intuitive: when the drone is too close, the door frame leaves the field of view and the drone sees through the opening into the room, so most pixels become distant—a *high* value therefore means *too close*, and the drone must back off. The metric is filtered by an EMA,

$$r_{\text{EMA}}^{(t)} = \alpha r^{(t)} + (1 - \alpha) r_{\text{EMA}}^{(t-1)}, \quad (3)$$

with $\alpha = 0.18$ and a target r^* within a ± 0.05 deadband; stabilization is declared after three consecutive in-band frames. Entry advances a fixed 1.8 m using the drone’s visual-odometry position command; the calibration profile is then switched to `room`. Before entry, the room number is read: the label plate is localized locally (Canny edges, aspect/area filtering), the crop is Base64-encoded and sent to the OCR

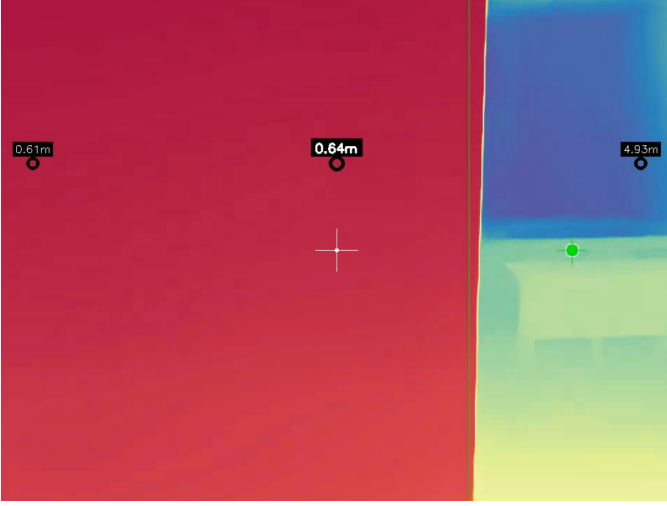


Fig. 2: Door detection on the depth map. The open door is isolated as a distant region flanked by sharp vertical depth edges corresponding to the door casing; appearance cues (handle, frame) are not required.

microservice, and the highest-scoring text with a valid 2–4-digit format is stored as `room_label`.

3) *Scanning, inspection and exit*: Two scan modes are offered. In *Simple* mode the drone measures the distance to the front wall, advances about a third of it, performs a full 360° rotation with brief pauses every 90° for stabilization, and returns symmetrically to the entry point. In *Complex* mode it measures the front, left, and right walls and then executes a five-segment perimeter crab covering a half-perimeter of the room—the most exhaustive coverage, at the cost of time and battery. Throughout the scan, the AI Analyzer runs in parallel: YOLO11n-Pose detects people with 17 COCO [23] keypoints, ByteTrack [24] maintains identities across frames, a purely geometric classifier assigns a posture (*standing, sitting, fallen, unknown*), and for each qualified person a cropped image is sent asynchronously to the medical microservice, which returns a visible-state estimate (STABLE, INJURED, CRITICAL, DECEASED, UNKNOWN). A second thread runs the fire/smoke detector, whose detections are logged as report events. On exit, the drone turns 205° (empirical yaw-drift compensation), re-acquires the door by a crab search, re-centers, re-stabilizes distance, and advances 1.8 m back into the corridor with active lateral correction. Every visited room yields a JSON record (OCR number, detected people with posture/medical state, hazards, timestamps) persisted to a local SQLite database and rendered directly in the web interface.

D. Autonomous stair ascent: the TRISTAR detector

The stair module, fully independent of the corridor module, drives the drone from the base of an interior staircase to the upper landing—a flat surface large enough to stabilize, with no visible steps. Its core is **TRISTAR** (TRI-Signal STair Ascent Recognition), which fuses three independent virtual sensors into a per-frame composite confidence score. Ascent starts

only if the composite score exceeds 0.52 with corroborating validation from all three sensors. Figs. 3 illustrate the three signals on a staircase versus a flat surface.

1) *Sensor 1 — horizontal Sobel*: On a 320×240 analysis image, the vertical gradient modulus $|G_y|$ responds strongly to each horizontal step edge. A trapezoidal mask excludes railings and side walls; the 1D vertical profile (row-wise mean) is Gaussian-smoothed, and peaks are detected by non-maximum suppression. A peak counts as a valid step only if its line covers at least 55% of the frame width. The score combines the uniformity U of inter-peak spacing (low CoV), the vertical coverage C , and the peak density D , penalizing scenes dominated by vertical gradients (likely doors or walls):

$$S_{\text{sobel}} = 0.40U + 0.35C + 0.25D. \quad (4)$$

2) *Sensor 2 — multi-scale Gabor*: Five Gabor kernels at $\theta = 90^\circ$ with wavelengths $\lambda \in \{14, 22, 32, 45, 65\}$ px cover steps from ~ 0.5 m to ~ 4 m. When depth is available, the wavelength is selected adaptively,

$$\lambda^*(d) = \frac{0.20}{d} f_y, \quad (5)$$

where 0.20 m is a standard step height, d the estimated metric distance, and f_y the vertical focal length. The key validation criterion is *edge-to-edge* coverage: every strongly responding line must span from the left to the right frame margin (with perspective-adjusted tolerance). Lines that fail are marked “red”, and

$$S_{\text{gabor}} = C_{\text{edge-to-edge}} (1 - r_{\text{red}}^{0.35}). \quad (6)$$

3) *Sensor 3 — monocular depth (DA2)*: Two depth properties are evaluated. The *global CoV* is large on steps ($\text{CoV} > 0.28$) and small on flat surfaces ($\text{CoV} < 0.12$). The *band monotonicity* splits the image into five horizontal bands: on a staircase viewed from below, the median depth must increase monotonically from the bottom band (near step) to the top band (far step). A single order inversion collapses the factor M to 0.05, two inversions to 0, which rejects flat walls or floors whose depth is large but non-monotonic. The score is

$$S_{\text{da2}} = \min(1, \text{normalize}(\text{CoV})) \cdot M. \quad (7)$$

4) *Composite score and ascent loop*: The composite confidence is the equally weighted mean,

$$\text{conf}_{\text{stairs}} = \frac{1}{3} (S_{\text{sobel}} + S_{\text{gabor}} + S_{\text{da2}}), \quad (8)$$

with an ascent threshold of 0.52. Once above threshold, the drone enters the ascent loop at a fixed 12 Hz, issuing three simultaneous RC commands per tick. The *forward* speed brakes proportionally with the median distance to the steps in the central region,

$$v_{\text{fb}}(d) = \begin{cases} 0 & d < d_{\text{min}}, \\ v_{\text{max}} \frac{d - d_{\text{min}}}{d_{\text{tgt}} - d_{\text{min}}} & d_{\text{min}} \leq d < d_{\text{tgt}}, \\ v_{\text{max}} & d \geq d_{\text{tgt}}, \end{cases} \quad (9)$$

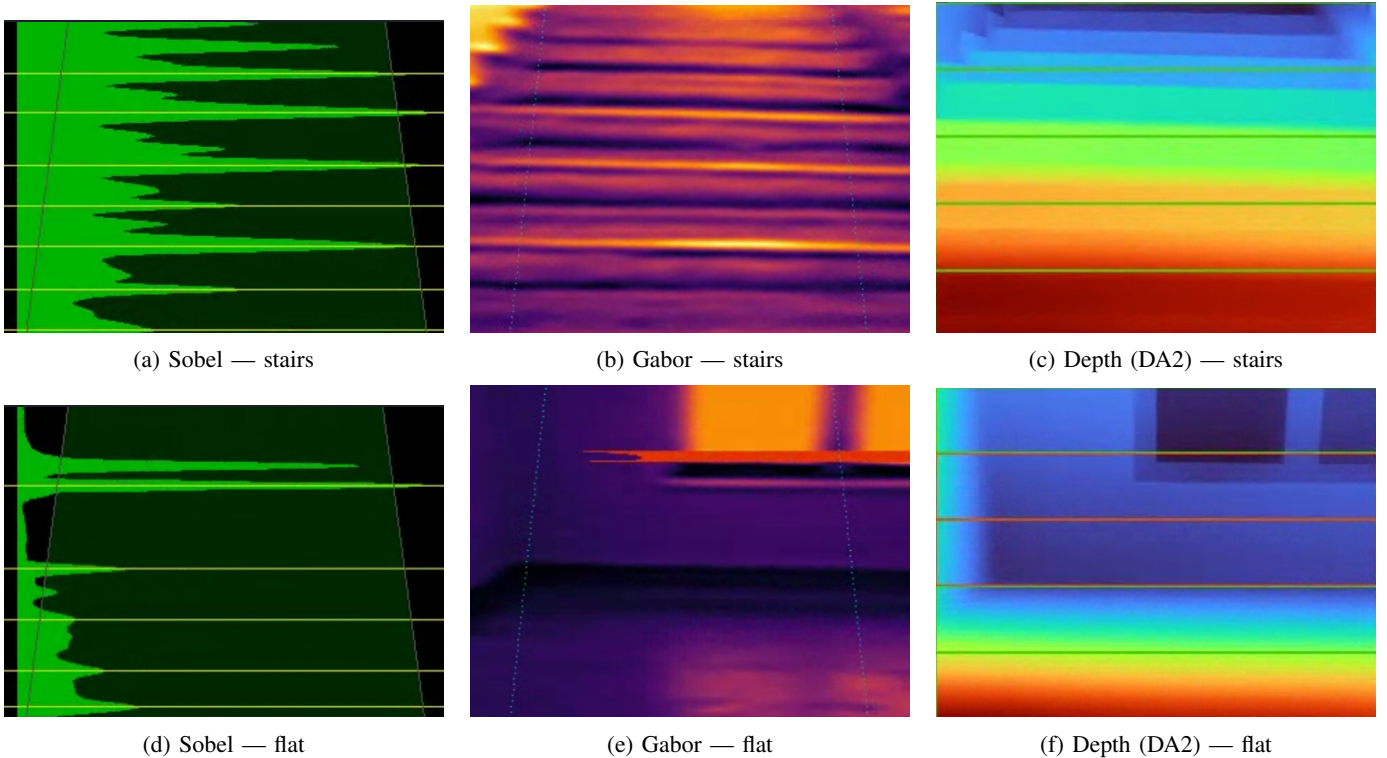


Fig. 3: The three virtual sensors of TRISTAR on a staircase (top) and on a flat surface (bottom). On stairs, Sobel yields regular horizontal peaks, Gabor yields consistent edge-to-edge lines, and the depth map is monotonic across horizontal bands; on a flat surface all three responses collapse.

with $d_{\min} = 0.7$ m, $d_{\text{tgt}} = 1.2$ m, $v_{\max} = 30$ cm/s. The *vertical* speed is proportional to the local slope estimated from the depth map by comparing the median depth of the upper band (d_{top}) and the lower band (d_{bot}),

$$\theta = \arctan(\Delta d / y_{\text{span}}), \quad v_{\text{ud}} = v_{\text{fb}} \tan \theta f_{\text{dist}}, \quad (10)$$

where $\Delta d = d_{\text{top}} - d_{\text{bot}}$ and y_{span} is the metric vertical extent of the frame. *Lateral* correction is derived from the left/right asymmetry of the Sobel step gaps. Ascent stops when all three sensors report “flat surface” for five consecutive frames (Sobel flat score ≥ 0.40 , no edge-to-edge Gabor lines, CoV < 0.12 with lost monotonicity); a short *pre-landing dash* then moves the drone clear of the last step edge. Safety layers include a 50 s per-flight timeout, a 20% battery floor, an operator abort, and continuous recording of every frame (raw + debug overlay) for post-flight analysis.

IV. EXPERIMENTAL RESULTS

Given the physical nature of the application, validation was organized on three levels: unit and integration tests on static datasets; reproducible flights with full video and RC logging, analyzed post-flight; and real end-to-end flights inside a university building. The backend ran on a laptop with an Intel Core i7, an NVIDIA RTX 3060 Mobile (6 GB VRAM), 16 GB RAM, Python 3.11, PyTorch 2.4, and CUDA 12.1. All flights used a single standard DJI Tello (720p camera, ~ 80 g, ~ 13 min per battery). Testing took place in a mock-up room

TABLE II: Calibrated depth-map error versus ground truth.

Profile	MAE	Mean rel. error	Std
room (0.5–3.0 m)	~ 0.18 m	8.5%	0.12 m
corridor (1.0–6.0 m)	~ 0.31 m	9.2%	0.24 m
Uncalibrated (raw metric DA2)	~ 0.85 m	27.4%	0.61 m

(for calibration) and in a university corridor (~ 2.4 m wide, 30+ m long, doors on both sides) and stairwell (standard steps, ~ 0.17 m rise, ~ 0.28 m run).

A. Video pipeline and depth accuracy

The pipeline meets its non-functional targets: ~ 30 FPS on the raw stream and ~ 10 – 12 Hz end-to-end (frame \rightarrow RC decision), with Depth Anything V2 (ViT-S) inferring at ~ 45 ms per frame on GPU and an end-to-end latency of ~ 85 – 100 ms (well below the 300 ms budget). The depth calibration was validated on 24 reference images across three contexts, with 5–8 manually selected reference points per image measured by a laser rangefinder (± 1 cm). As Table II shows, empirical calibration reduces the mean relative error from 27.4% (raw metric DA2) to below 10% for both profiles. This precision is sufficient for all control decisions, which use distance *intervals* (e.g. 1.7–6.0 m for door thresholds, 0.7–1.2 m for the ascent braking zone) rather than precise absolute values (Fig. 4).

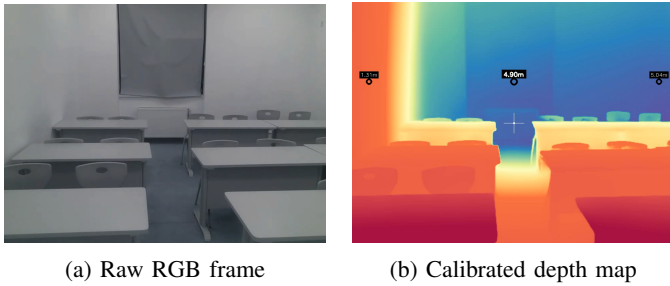


Fig. 4: A raw frame (left) and its corresponding calibrated depth map (right), the source of all derived navigation metrics.

TABLE III: Door-detection filter ablation (offline validation set).

Metric	All filters	No edge	No content	Contour only
True positives	128	134	130	138
False positives	9	47	28	91
Precision	0.93	0.74	0.82	0.60
Recall	0.90	0.94	0.92	0.97
F1	0.91	0.83	0.86	0.74

B. Corridor navigation

1) *Door detection*: The algorithm was evaluated offline on 142 positive and 168 negative frames extracted from 8 recordings. With all filters active it reaches a precision of 0.93, a recall of 0.90, and an F1-score of 0.91 (Table III). The vertical-edge filter is by far the most effective at suppressing false positives, cutting them from 47 to 9—confirming the core hypothesis that a real door is characterized more by its vertical casing edges than by the mere presence of a distant region.

To characterize its limits, the real detector was run on photographs of difficult scenes, brought to the drone frame format. Two behaviors emerge (Fig. 5). First, *robustness to appearance traps*: a wardrobe and a mirror both produce a distant region in the depth map, but without a real casing—their margins are no closer than their centers, so R stays far below threshold (0.05 and 0.38) and both are correctly rejected. The detection thus rests on the geometric structure of the opening, not on appearance. Second, *genuine limitations*: a glass window (Fig. 5b) has exactly the depth profile of an opening, with clear lateral edges ($R = 6.97$), which a purely monocular method cannot distinguish from a door; and under very low light (Fig. 5c) the depth map becomes too smooth, the real casing edges vanish ($R = 0.10$), and a real door is missed. Both failures stem from the monocular depth sensor, not from the detection logic—and in operation the presence of a real door is later confirmed by OCR of the plate on entry.

2) *Closed-loop behavior*: Across 12 end-to-end flights, lateral centering finished within the ± 25 px tolerance in 11 of 12 cases (the single miss still entered without collision). The distance controller uses `full_frame_blue_ratio` filtered by the EMA ($\alpha = 0.18$), with a target and a ± 0.05 deadband, declaring stabilization after three consecutive in-band frames. Fig. 6 shows a real door entry extracted from

TABLE IV: Individual virtual sensors versus the fused TRISTAR score, on the *stairs* and *landing* classes.

Sensor	Stairs		Landing	
	Precision	Recall	Precision	Recall
Sobel only	0.78	0.85	0.65	0.59
Gabor only	0.82	0.79	0.71	0.68
DA2 only	0.74	0.81	0.83	0.77
Sobel + Gabor	0.87	0.86	0.69	0.63
Sobel + DA2	0.83	0.86	0.82	0.76
Gabor + DA2	0.85	0.84	0.83	0.78
TRISTAR	0.92	0.88	0.86	0.81

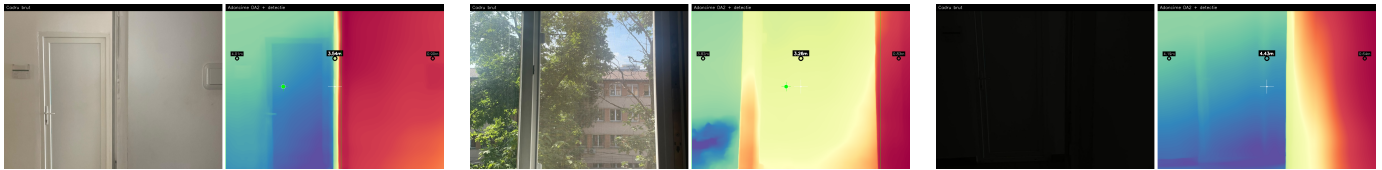
the mission logs: a noise spike in the raw signal is absorbed by the EMA, which stays smooth and converges within the deadband without reversing the drone’s direction. Across the seven logged door entries, the EMA variation stayed small (median ~ 0.03), confirming the stability of the filtering; the single large excursion (0.29) corresponds to an entry started from a large distance. Room entry (1.8 m advance) succeeded in 12/12 cases without touching the door frame. The Simple scan succeeded in 12/12 flights (~ 42 s, 1.6 detected people on average); the Complex scan succeeded in 10/12 (~ 60 s, 3.2 people), the two failures caused by cumulative yaw drift after two consecutive 90° rotations—a known Tello limitation addressed in future work through IMU gravity-vector compensation. All 12 missions produced a valid report, OCR read the room number correctly in 82% of automatic in-flight attempts, and every effectively visible person was qualified and reported.

C. Stair ascent: the ablation study

The contribution of each virtual sensor was assessed in two stages: an *offline* evaluation of detection quality and a *closed-loop* study on real flights with each signal isolated and each combination active.

Offline detection. On 220 frames labeled *stairs visible* (118), *landing* (54), and *other* (48), Table IV reports the per-sensor and fused precision/recall. Full fusion clearly dominates, especially in reducing false positives: Sobel false positives on walls with doors (interpreted as horizontal lines) are removed by Gabor, while Gabor false positives on textiles or tiled floors are removed by the low-CoV DA2 signal on flat regions. TRISTAR reaches a precision of 0.92 and a recall of 0.88 on the *stairs* class, and 0.86/0.81 on the *landing* class—higher than any single sensor or pair.

Closed-loop flights. To observe the effect of each signal on in-loop behavior, the detector was run in seven configurations—each signal alone, the three pairs, and full fusion—with four ascent flights per configuration (28 flights total). Table V summarizes the outcomes and the dominant failure mode of each partial configuration. The result is unambiguous: no partial configuration matches the reliability of full fusion, and each missing signal induces a characteristic failure. Without depth (Sobel, Gabor, Sobel+Gabor) the drone is “blind” to the end of the ramp and either overshoots into the ceiling/wall or lands prematurely; DA2 alone is fooled by window sills that mimic a stair depth profile and never



(a) Partial door, correctly detected ($R = 52.75$) (b) Window, false positive ($R = 6.97$) (c) Low light, false negative ($R = 0.10$)

Fig. 5: Door-detection failure analysis. The edge ratio R (threshold 1.20) decides acceptance. Appearance traps such as wardrobes and mirrors are rejected; the two residual failures—glass and very low light—are inherent to monocular depth, not to the detection logic.

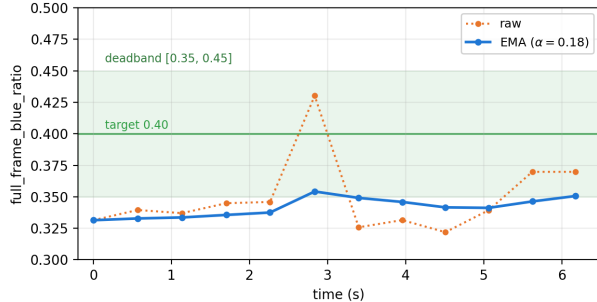


Fig. 6: Real evolution of `full_frame_blue_ratio` (raw vs. EMA) during a door entry. The EMA absorbs the raw-signal noise spike and converges within the deadband, preventing a spurious direction reversal.

TABLE V: Closed-loop ablation on real flights (4 flights per configuration).

Configuration	Success	Dominant failure mode
Sobel	2/4	Reads steps but, lacking depth, overshoots the landing or lands early.
Gabor	2/4	Recognizes the repetitive structure but rises excessively past the last step.
DA2	0/4	Depth monotonicity fooled by windows/sills; landing not recognized.
Sobel + Gabor	1/4	Strong “up” cue but no depth \Rightarrow climbs toward the ceiling.
Sobel + DA2	2/4	Works but unstable: useless lifts and a false landing when steps leave view.
Gabor + DA2	1/4	No per-step “up” cue \Rightarrow too many forward commands, overshoots.
TRISTAR	4/4	Full fusion: every signal covers the others’ weaknesses.

succeeds; removing Sobel (Gabor+DA2) drops the per-step “up” cue and the drone advances past the landing. Only TRISTAR succeeds in all four flights, each signal covering the others’ blind spots. Figs. 7 show, for the three pairs and for full fusion, the temporal evolution of the signals during a representative flight.

Failure-case analysis. Running the real detector on static photographs of deceptive scenes (Table VI) confirms the role of fusion. On a railing and on a shelf, Sobel and Gabor respond strongly to the repetitive horizontal lines (a per-signal false positive), but the DA2 component (0.00) pulls the

TABLE VI: Per-signal scores and the TRISTAR decision (ascent if ≥ 0.52).

Scene	Truth	Sobel	Gabor	DA2	Score	OK?
Stairs, low light	stairs	0.80	1.00	0.99	0.93	✓
Partial stairs (left)	stairs	0.75	1.00	1.00	0.91	✓
Stairs + obstacle	stairs	0.00	1.00	0.00	0.25	–
Partial stairs (right)	stairs	0.00	1.00	0.00	0.25	–
Railing	non	0.68	1.00	0.00	0.49	✓
Shelf	non	0.85	0.69	0.00	0.47	✓

composite score below threshold, correctly rejecting the scene (the *Railing* row of Table VI). Conversely, the system misses a scene (false negative) when the steps are not geometrically visible: an obstacle in front of the staircase or a field of view with too few steps simultaneously nullifies Sobel and DA2, and Gabor alone cannot reach the threshold. These modes confirm that detection depends on the geometric visibility of the steps, while robustness to deceptive structures is provided precisely by the fusion of the three signals, not by any single detector.

For a typical ramp (12 steps, ~ 3.4 m long, ~ 2.05 m high), the drone climbed in ~ 19 s on average, at an effective vertical speed of ~ 0.11 m/s—below the drone’s theoretical maxima, reflecting the conservative control policy (braking near the steps, five-frame confirmation for landing detection).

D. Auxiliary AI components

Posture estimation from YOLO11-Pose keypoints, evaluated on 96 frames, reached a weighted accuracy of $\sim 87\%$, with the operationally critical *fallen* class at 83%. OCR of room numbers reached 85% overall (92% on favorable-angle frames, 82% on automatic in-flight frames), with failures traced to strong backlight, capture angle, and non-standard plate fonts. The Gemini medical triage returned an acceptable state (STABLE/UNKNOWN) in 22 of 24 cases, with the two over-classifications (INJURED on a slightly tilted posture) illustrating the tendency of large models to over-interpret subtle visual cues; the mean response time was ~ 1.6 s, small enough to be included in the report without delaying post-processing. The fire/smoke detector reached 8/8 true positives and 1/12 false positives on reference images and runs as a separate reporting thread that does not affect navigation.

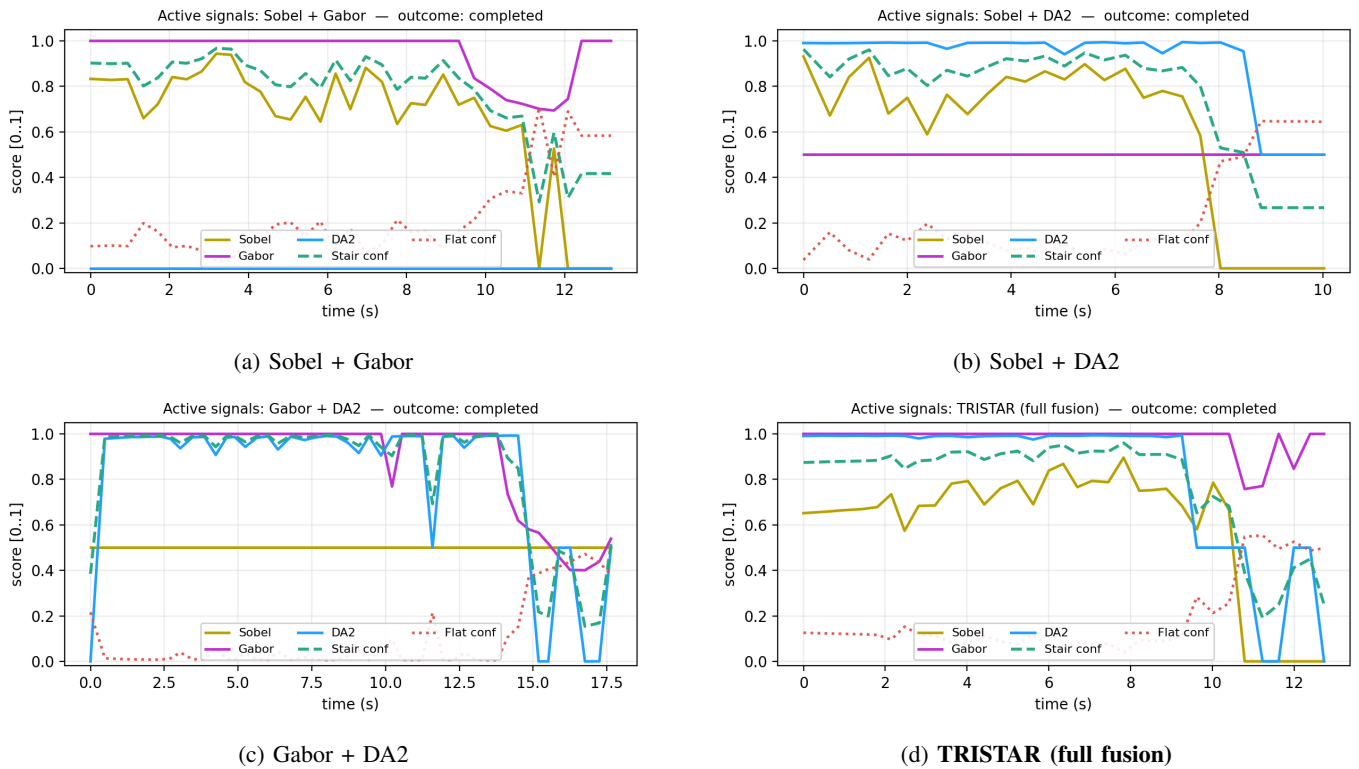


Fig. 7: Temporal evolution of the signals during a representative ascent for the three pairwise configurations and for full fusion. In the pairs, a missing modality lets one signal drift; under full TRISTAR fusion (d) all signals remain high and concordant during the climb and jointly collapse (with the “flat” confidence rising) exactly at the landing.

TABLE VII: Summary of results against implicit targets.

Component / metric	Target	Achieved	
Raw stream FPS	≥ 25	~ 30	✓
Depth stream FPS	≥ 10	$\sim 10\text{--}12$	✓
End-to-end latency	< 300 ms	$\sim 85\text{--}100$ ms	✓
Calibrated depth error (room)	$< 15\%$	$\sim 8.5\%$	✓
Door detection F1 (offline)	> 0.85	0.91	✓
Corridor flight success	$> 80\%$	12/12	✓
Stair detection F1 (offline)	> 0.85	~ 0.90	✓
Stair ascent success (flight 1)	$> 80\%$	8/8	✓
Room-number OCR accuracy	$> 80\%$	85%	✓
Posture accuracy	$> 75\%$	$\sim 87\%$	✓

E. Summary

Table VII consolidates the main results against their implicit targets. All targets are met or exceeded, and the two autonomous subsystems operate independently on real flights. The identified limitations—cumulative yaw drift over multiple rotations, dependence on Gemini for medical triage, and the absence of a global map—are known, documented, and form the direct agenda of future iterations.

V. CONCLUSION

This paper set out from a deliberately practical question—*how much can be done autonomously with a cheap commercial drone that carries no dedicated sensors*—and answered it

concretely. We showed that modern monocular vision, combined with classical computer-vision tools and a clean modular design, is enough to let a sub-150 EUR drone autonomously explore a building corridor, enter rooms, read their labels, detect and triage people, and climb a staircase—tasks that until now demanded either a human operator or an expensive sensor suite. The central technical result is that the division of labor between paradigms pays off: geometric structure (open doors, stair steps) is recovered elegantly from a calibrated monocular depth map and classical filters, without training a dedicated detector, while semantic understanding (people, fire, smoke, medical state) is delegated to neural models. Empirical calibration alone brings the relative depth error from 27.4% to below 10%, enough for every control decision in the system, and the door detector reaches an F1-score of 0.91 while correctly rejecting appearance traps such as wardrobes and mirrors.

The clearest embodiment of this philosophy is TRISTAR. The ablation study is categorical: no single virtual sensor, and no pair of them, matches the reliability of the three-way fusion—each isolated modality carries a characteristic, reproducible failure mode, and only the composite score succeeds in every flight. Structural cues supply the per-step signal, texture analysis supplies robustness to perspective, and monocular depth supplies the geometric validation that recognizes the landing and refuses the traps that fool the other two. It is

precisely because each sensor is individually fragile that their fusion is strong.

Two honest limitations frame these results. The system builds no persistent (SLAM) map, so each mission is geometrically independent, and the corridor and stair behaviors are still operated separately rather than composed into a single continuous mission. Neither limitation is fundamental: both follow largely from the chosen hardware, not from the software stack, which is in principle portable to any drone exposing a video feed and RC control. The most promising directions are therefore a monocular-SLAM layer for a persistent building map, a transition state that chains stair ascent into upper-floor corridor exploration, on-device medical triage to remove the cloud dependency, and a migration to a more capable platform for multi-drone coordinated exploration.

More broadly, this work illustrates a wider trend in applied robotics: as vision models grow more capable and more efficient, the total cost of a drone capable of genuine indoor autonomy keeps falling, and the accessibility of such systems keeps rising. A capability that today requires an 11,000 USD platform is, increasingly, a matter of software running on an 80-gram toy. If a commodity camera and a few classical filters can already guide a drone up a dark stairwell toward the people who need to be found, the question worth carrying forward is no longer whether low-cost autonomy is possible, but how far it can be pushed—and how many lives that reach might one day help save.

REFERENCES

- [1] L. Yang, B. Kang, Z. Huang, Z. Zhao, X. Xu, J. Feng, H. Zhao, “Depth Anything V2,” *arXiv:2406.09414*, 2024.
- [2] Skydio Inc., “Skydio X10 / Skydio 2+ technical specifications,” <https://www.skydio.com>.
- [3] DJI, “DJI Matrice 30 / Mavic 3 Enterprise specifications,” <https://www.dji.com>.
- [4] Modal AI Inc., “Voxl 2 / Starling 2 developer documentation,” <https://www.modalai.com>.
- [5] D. Fuentes, “djitelopy: DJI Tello drone Python interface using the official Tello SDK,” GitHub repository, <https://github.com/damiafuentes/DJITelloPy>.
- [6] R. Ranftl, K. Lasinger, D. Hafner, K. Schindler, V. Koltun, “Towards Robust Monocular Depth Estimation: Mixing Datasets for Zero-shot Cross-dataset Transfer,” *IEEE TPAMI*, 2020.
- [7] S. F. Bhat, R. Birkl, D. Wofk, P. Wonka, M. Müller, “ZoeDepth: Zero-shot Transfer by Combining Relative and Metric Depth,” *arXiv:2302.12288*, 2023.
- [8] N. Silberman, D. Hoiem, P. Kohli, R. Fergus, “Indoor Segmentation and Support Inference from RGBD Images,” *ECCV*, 2012.
- [9] A. Geiger, P. Lenz, R. Urtasun, “Vision meets robotics: The KITTI dataset,” *IJRR*, vol. 32, no. 11, pp. 1231–1237, 2013.
- [10] Z. Teed, J. Deng, “DROID-SLAM: Deep Visual SLAM for Monocular, Stereo, and RGB-D Cameras,” *NeurIPS*, 2021.
- [11] Z. Teed, L. Lipson, J. Deng, “Deep Patch Visual Odometry,” *NeurIPS*, vol. 36, 2023.
- [12] M. Arduengo, C. Torras, L. Sentis, “Robust and adaptive door operation with a mobile robot,” *Intelligent Service Robotics*, vol. 14, pp. 409–425, 2021.
- [13] J. G. Ramôa, L. A. Alexandre, S. Mogo, “Real-Time 3D Door Detection and Classification on a Low-Power Device,” *IEEE ICARSC*, 2020.
- [14] J.-M. Park et al., “Indoor/Outdoor Transition Recognition Based on Door Detection,” *19th Int. Conf. on Ubiquitous Robots (UR)*, 2022, pp. 384–387.
- [15] X. Lin et al., “A Context-Aware Doorway Alignment and Depth Estimation Algorithm for Assistive Wheelchairs,” *Computers*, vol. 14, no. 7, p. 284, 2025.
- [16] DARPA, “Subterranean Challenge,” program page, <https://www.darpa.mil/program/darpa-subterranean-challenge>.
- [17] D. Gabor, “Theory of communication,” *Journal of the IEE*, vol. 93, no. 26, pp. 429–457, 1946.
- [18] S. Ramírez, “FastAPI: Modern, fast web framework for building APIs with Python,” documentation, <https://fastapi.tiangolo.com>.
- [19] G. Jocher, A. Chaurasia, J. Qiu, “YOLO11 by Ultralytics,” GitHub repository, 2024.
- [20] G. Jocher, A. Chaurasia, J. Qiu, “YOLOv8 by Ultralytics,” GitHub repository, 2023.
- [21] JaiedAI, “EasyOCR: Ready-to-use OCR with 80+ supported languages,” GitHub repository, <https://github.com/JaiedAI/EasyOCR>.
- [22] Google DeepMind, “Gemini: A Family of Highly Capable Multimodal Models,” technical report, 2024.
- [23] T.-Y. Lin et al., “Microsoft COCO: Common Objects in Context,” *ECCV*, 2014.
- [24] Y. Zhang et al., “ByteTrack: Multi-Object Tracking by Associating Every Detection Box,” *ECCV*, 2022.